

Article

Structure of Analytical and Numerical Wave Solutions for the Nonlinear (1 + 1)-Coupled Drinfel'd–Sokolov–Wilson System Arising in Shallow Water Waves

Sumayah Hamzah Alhejaili and Abdulghani Alharbi * 

Department of Mathematics, College of Science, Taibah University, Al-Madinah al-Munawwarah 42353, Saudi Arabia; sumayah.hamzah11@gmail.com

* Correspondence: arharbi@taibahu.edu.sa

Abstract: In this article, we successfully obtain novel solutions for the coupled Drinfel'd–Sokolov–Wilson DSW system utilizing various methods. These include soliton solutions characterized by hyperbolic, rational, and trigonometric functions. Specifically, the generalized exponential rational function method (GERFM) and a modified version of the new Kudryashov method (MVNK) are employed to derive diverse soliton solutions for the system. Additionally, we demonstrate numerical solutions for the coupled Drinfel'd–Sokolov–Wilson system using adaptive moving mesh and uniform mesh methods. Also, we study the stability and error analysis of the numerical schemes. To validate the accuracy and reliability of the exact solutions obtained through analytical methods, we compare them with the numerical solutions both analytically and graphically. The techniques presented in this article are deemed suitable and acceptable and can be effectively applied to solve other nonlinear evolution systems.

Keywords: coupled Drinfel'd–Sokolov–Wilson system; exact solution; numerical solution; waves; adaptive moving mesh method; uniform mesh; monitor function

MSC: 35A24; 35B35; 35Q51; 35Q92; 65N06; 65N40; 65N45; 65N50



Citation: Alhejaili, S.H.; Alharbi, A.

Structure of Analytical and Numerical Wave Solutions for the Nonlinear (1 + 1)-Coupled Drinfel'd–Sokolov–Wilson System Arising in Shallow Water Waves. *Mathematics* **2023**, *11*, 4598. <https://doi.org/10.3390/math11224598>

Academic Editor: Tholang Mokhele

Received: 10 October 2023

Revised: 4 November 2023

Accepted: 5 November 2023

Published: 9 November 2023



Copyright: © 2023 by the authors. Licensee MDPI, Basel, Switzerland. This article is an open access article distributed under the terms and conditions of the Creative Commons Attribution (CC BY) license (<https://creativecommons.org/licenses/by/4.0/>).

1. Introduction

Partial differential equations (PDEs) are powerful tools for modeling and analyzing various phenomena in nature and physics. These include plasma physics, population dynamics, fluid and gas flow, electromagnetic fields, wave propagation in liquids, radiation, optical fibers, heat transfer, and other processes [1–6]. PDEs offer an effective and successful approach to studying and comprehending these phenomena. Understanding soliton propagation is critical for grasping important oceanic phenomena, like how nonlinear waves move in shallow or deep seas, how transverse waves move in shallow water, how magneto-hydrodynamic waves move in plasma, and how phonon packets behave in nonlinear crystals. The study of PDEs allows us to better understand the future behavior of various phenomena accurately by utilizing exact and numerical solutions [7–10]. It is essential to explore the precise solutions of nonlinear phenomena to gain insight into their long-term behavior. As a result, the development of systematic methods for deriving analytical solutions to PDEs has become a captivating and widely studied area of research among scholars. There are various techniques available to obtain analytical solutions to partial differential equations. Some of these techniques include the improved Kudryashov approach, the generalized direct algebraic strategy, the first integral approach, and many others. To learn more about these techniques and the analytical solutions they generate, one can refer to references [11–16].

In this study, we investigate a coupled system of nonlinear partial differential equations representing a nonlinear (1 + 1)-coupled Drinfel'd–Sokolov–Wilson system [17]

$$\begin{cases} \Gamma_t + a\Psi\Psi_x = 0, \\ \Psi_t + b\Psi_{xxx} + c\Gamma\Psi_x + d\Psi\Gamma_x = 0, \end{cases} \quad (1)$$

where x and t are the space variable and time variable, both of which are, respectively, independent, and the dependent variables are Γ, Ψ . Finding solutions for the shallow water equations, also known as DSW equations, has been a significant area of research. These equations are versatile and can be used to model various water flow situations that involve gravity and shear stress. They are crucial for simulating significant events in engineering and physics, such as floods, dam breaks, and flows through vegetated regions. Therefore, much effort has been put into understanding and solving these equations, which are critical in various scientific and engineering applications. Various studies have analyzed the the coupled Drinfel'd–Sokolov–Wilson system for its numerical and exact solutions. For example, direct algebraic techniques, the Adomian decomposition method, the variational approach, and others, have been used to thoroughly study the the coupled Drinfel'd–Sokolov–Wilson system [18–21]. Recently, there has been much interest in investigating the fractional-order coupled Drinfel'd–Sokolov–Wilson system using a variety of techniques, including the use of conformable derivatives, the homotopy perturbation method, the $\frac{G}{G}$ expansion, the F-expansion method, tanh and extended tanh methods, the truncated Painlevé method, and the exp-function method. Furthermore, the discrimination system for polynomial and Jacobi elliptical functions has been explored [22–26]. In [27], the finite difference method was used to obtain numerical solutions for the coupled Drinfel'd–Sokolov–Wilson system. Previous studies on Equation (2) have predominantly concentrated on obtaining numerical solutions without actively addressing or reducing the resulting errors. In contrast, our study successfully reduced errors and received accurate numerical solutions for system (1).

This paper is motivated by the recent advancements discussed in the literature review. The primary objective of this study is to utilize the GERFM technique and the MVNK technique to develop various traveling wave solutions for the coupled Drinfel'd–Sokolov–Wilson system. The proposed methods have distinct advantages, which are listed below. These methods present a diverse range of reliable traveling wave solutions expressed in trigonometric, hyperbolic, and rational forms. These solutions act as dependable tools in interpreting intricate phenomena and gaining insights into their underlying dynamics. In addition, this paper aims to apply the adaptive moving mesh and uniform mesh method to system (1) in order to obtain its numerical solutions. It is worth noting that the initial condition for the numerical scheme is derived from the constructed exact solutions. The primary concept behind the employed numerical method is to distribute the mesh points in the solution curvature regions. While many researchers focus on analytically finding traveling wave solutions for the coupled Drinfel'd–Sokolov–Wilson system, only a few scientists have explored the numerical solutions to this problem with a high level of precision, aiming to minimize the error. The adaptive moving mesh approach ensures that the points are evenly distributed in areas with high error, effectively reducing the error. This technique, which is not commonly available in most numerical algorithms, significantly improves the accuracy of the results. To ensure the accuracy of the solutions, comparing the exact and numerical solutions is crucial. While some studies focus solely on finding exact solutions, this study goes a step further by comparing the exact and numerical solutions to ensure their accuracy and correctness.

The structure of this paper is as follows: Section 2 introduces the analytic solution for Equation (5). Section 3 focuses on presenting the numerical solution for system (1) using both fixed mesh and adaptive moving mesh techniques. This section also includes the results and subsequent discussion. Finally, Section 4 highlights the most significant findings discovered in this study.

2. Exact Solutions of the Coupled Drinfel’d–Sokolov–Wilson System

This section introduces the MVNK and the GERFM methods for finding soliton solutions of nonlinear evolution equations.

$$P_1(\Psi, \Psi_x, \Psi_t, \Psi_{xx}, \Psi_{xxx}, \Gamma, \Gamma_x, \dots) = 0, \tag{2}$$

where $\Psi = \Psi(x, t)$ is an unknown function, P_1 is a polynomial of $\Psi(x, t)$, and various partial derivatives are involved in Equation (2). The wave transformation is applied as follows:

$$\Psi(x, t) = \psi(\zeta), \quad \Gamma(x, t) = \Gamma(\zeta), \quad \zeta = x - st,$$

into Equation (2) to reduce Equation (2) into an ordinary differential equation (ODE) expressed as

$$P_2(\psi, \psi, \psi_\zeta, \psi_{\zeta\zeta}, \psi_{\zeta\zeta\zeta}, \Gamma, \Gamma_\zeta, \dots) = 0,$$

after substituting the traveling wave into the system (1), we get the following expression:

$$-s\Gamma_\zeta + a\Psi\Psi_\zeta = 0, \tag{3}$$

from Equation (3), we have

$$\Gamma = \frac{a}{2s}\Psi^2, \tag{4}$$

by substituting Equation (4) into system (1), the system is converted into a single equation

$$\Psi_t + b\Psi_{xxx} + \alpha\Psi^2\Psi_x = 0, \tag{5}$$

since $(\frac{ca}{2s} + \frac{ad}{s}) = \alpha$, Equation (5) reduces to an ODE given by

$$-s\Psi + b\Psi_{\zeta\zeta} + \frac{1}{3}\alpha\Psi^3 = 0, \tag{6}$$

balancing $\Psi_{\zeta\zeta}$ with Ψ^3 in Equation (6) calculates the value of $N = 1$.

2.1. The MVNK Method

To apply MVNK [28], Equation (2) can be expressed as follows:

$$\psi(\zeta) = z_0 + \sum_{j=1}^N \left(\frac{\sigma(\zeta)}{1 + \sigma^2(\zeta)} \right)^{j-1} \left(z_j \frac{\sigma(\zeta)}{1 + \sigma^2(\zeta)} + c_j \frac{1 - \sigma^2(\zeta)}{1 + \sigma^2(\zeta)} \right), \quad z_j \neq 0 \text{ or } c_j \neq 0, \tag{7}$$

where the values of z_0, z_j , and c_j for $j = 1, 2, 3, \dots, N$ are to be later determined. The following function is satisfied by $\sigma(\zeta)$, and N is the homogeneous balance of numbers

$$\sigma(\zeta) = \frac{1}{(U - Y) \sinh(\zeta) + (U + Y) \cosh(\zeta)}, \tag{8}$$

the Jacobi equation is satisfied by the following expression:

$$\sigma'(\zeta)^2 = \sigma^2(\zeta)(1 - 4UY\sigma^2(\zeta)),$$

the exact solutions of (5) are

$$\psi(\zeta) = z_0 + z_1 \frac{\sigma(\zeta)}{1 + \sigma^2(\zeta)} + c_1 \frac{(1 - \sigma^2(\zeta))}{1 + \sigma^2(\zeta)}, \tag{9}$$

the constants z_0, z_1 , and c_1 in Equation (9) are to be determined, such that $z_1 \neq 0$ or $c_1 \neq 0$, and $\sigma(\zeta)$ satisfies Equations (7) and (8). By substituting Equation (9) into Equation (6) and

rearranging the terms, we obtain a system of algebraic equations. Solving this system gives us the following soliton solutions.

Family 1: If we set $Y = 0$ in Equation (8), we have

Cluster-1: When $z_0 = 0, z_1 = \mp \frac{4\sqrt{3}b}{\sqrt{ac+2ad}}, c_1 = 0, s = b$, exact traveling wave solutions are provided by

$$\Psi_1(x, t) = \mp \frac{4\sqrt{3} b U}{\sqrt{a(c + 2d)}((U^2 + 1) \cosh(bt - x) - (U^2 - 1) \sinh(bt - x))},$$

$$\Gamma_1(x, t) = \frac{24 b U^2}{(c + 2d)((U^2 + 1) \cosh(bt - x) - (U^2 - 1) \sinh(bt - x))^2}.$$

If we set $U^2 = 1$ in Equation (8), then we have

$$\Psi_2(x, t) = \mp \frac{2\sqrt{3} b \operatorname{sech}(bt - x)}{\sqrt{a(c + 2d)}},$$

$$\Gamma_2(x, t) = \frac{6 b \operatorname{sech}^2(bt - x)}{c + 2d}.$$

If we set $U^2 = -1$ in Equation (8), then we have

$$\Psi_3(x, t) = \mp \frac{2i\sqrt{3} b \operatorname{csch}(bt - x)}{\sqrt{a(c + 2d)}},$$

$$\Gamma_3(x, t) = -\frac{6 b \operatorname{csch}^2(bt - x)}{c + 2d}.$$

Cluster-2: When $z_0 = 0, z_1 = 0, c_1 = \mp \frac{2\sqrt{6}b}{\sqrt{ac+2ad}}, s = -2b$, exact traveling wave solutions are provided by

$$\Psi_4(x, t) = \mp \frac{2\sqrt{6} b (U^2 (\cosh[2bt + x] + \sinh[2bt + x])^2)^{-1}}{\sqrt{a(c + 2d)}((U \sinh(2bt + x) + U \cosh(2bt + x))^{-2} + 1)},$$

$$\Gamma_4(x, t) = -\frac{6 b ((U^2 (\sinh(2bt + x) + \cosh(2bt + x))^2)^{-1} - 1)^2}{(c + 2d)((U \sinh(2bt + x) + U \cosh(2bt + x))^{-2} + 1)^2}.$$

If we set $U^2 = 1$ in Equation (8), then we have

$$\Psi_5(x, t) = \mp \frac{2\sqrt{6} b \tanh(2bt + x)}{\sqrt{a(c + 2d)}},$$

$$\Gamma_5(x, t) = -\frac{6 b \tanh^2(2bt + x)}{c + 2d}.$$

If we set $U^2 = -1$ in Equation (8), then we have

$$\Psi_6(x, t) = \mp \frac{2\sqrt{6} b \coth(2bt + x)}{\sqrt{a(c + 2d)}},$$

$$\Gamma_6(x, t) = -\frac{6 b \coth^2(2bt + x)}{c + 2d}.$$

Family 2: If we set $Y = \frac{-1}{2U}$ in Equation (8), we obtain

Cluster-1: When $z_0 = \pm \frac{4\sqrt{3}b}{\sqrt{a(c+2d)}}$, $z_1 = 0$, $c_1 = \mp \frac{4\sqrt{3}b}{\sqrt{ac+2ad}}$, $s = 4b$, exact traveling wave solutions are provided by

$$\Psi_7(x, t) = \pm \frac{32\sqrt{3}bU^2}{\sqrt{a(c+2d)}((1-4U^4)\sinh(8bt-2x) + (4U^4+1)\cosh(8bt-2x))},$$

$$\Gamma_7(x, t) = \frac{384bU^4}{(c+2d)((1-4U^4)\sinh(8bt-2x) + (4U^4+1)\cosh(8bt-2x))^2}.$$

If we set $U^2 = \frac{1}{2}$ in Equation (8), then we have

$$\Psi_8(x, t) = \pm \frac{8\sqrt{3} b \operatorname{sech}(8bt - 2x)}{\sqrt{a(c + 2d)}},$$

$$\Gamma_8(x, t) = \frac{24 b \operatorname{sech}^2(8bt - 2x)}{c + 2d}.$$

If we set $U^2 = -\frac{1}{2}$ in Equation (8), then we have

$$\Psi_9(x, t) = \mp \frac{8\sqrt{3} b \operatorname{sech}(8bt - 2x)}{\sqrt{a(c + 2d)}},$$

$$\Gamma_9(x, t) = \frac{24 b \operatorname{sech}^2(8bt - 2x)}{c + 2d}.$$

2.2. The GERFM Method

To apply GERFM [29,30], Equation (2) can be expressed as follows:

$$\psi(\zeta) = r_0 + \sum_{j=1}^N r_j Y(\zeta)^j + \sum_{j=1}^N a_j Y(\zeta)^{-j}, \tag{10}$$

the $Y(\zeta)$ function satisfies the following differential equation:

$$Y(\zeta) = \frac{v_1 \exp(k_1 \zeta) + v_2 \exp(k_2 \zeta)}{v_5 \exp(k_3 \zeta) + v_6 \exp(k_4 \zeta)}, \tag{11}$$

where $v_1, v_2, v_5, v_6, k_1, k_2, k_3$, and k_4 are complex (or real) constants. According to the GERFM, with $N = 1$, the solutions of Equation (5) are

$$\psi(\zeta) = r_0 + r_1 Y(\zeta) + a_1 Y(\zeta)^{-1}, \tag{12}$$

the constants r_0, r_1 , and a_1 in Equation (12) are to be determined, such that $r_1 \neq 0$ or $a_1 \neq 0$, and $Y(\zeta)$ satisfies Equations (10) and (11). By substituting Equation (12) into Equation (6) and rearranging the terms, we obtain a system of algebraic equations. Solving this system gives us the following soliton solutions.

Family 1: When $v = [1, -1, 1, 1]$ and $k = [-1, 1, -1, 1]$, Equation (11) can be expressed as

$$Y(\zeta) = -\tanh(\zeta). \tag{13}$$

The algebraic system is obtained by substituting Equation (13) into Equation (12) and then inserting the result into Equation (6). The solutions are as follows:

Cluster-1: When $r_0 = 0, r_1 = 0, a_1 = \mp \frac{2\sqrt{6}b}{\sqrt{ac+2ad}}, s = -2b$, the exact traveling wave solutions are provided by

$$\Psi_{10}(x, t) = \pm \frac{2\sqrt{6} b \coth(2bt + x)}{\sqrt{a(c + 2d)}},$$

$$\Gamma_{10}(x, t) = -\frac{6b \coth^2(2bt + x)}{c + 2d}.$$

Cluster-2: When $r_0 = 0, r_1 = \mp \frac{4\sqrt{3}b}{\sqrt{-ac-2ad}}, a_1 = \pm \frac{4\sqrt{3}b}{\sqrt{-a(c+2d)}}, s = 4b$, the exact traveling wave solutions are provided by

$$\Psi_{11}(x, t) = \pm \frac{8\sqrt{3} b \operatorname{csch}(8bt - 2x)}{\sqrt{-a(c + 2d)}},$$

$$\Gamma_{11}(x, t) = -\frac{24 b \operatorname{csch}^2(8bt - 2x)}{c + 2d}.$$

Cluster-3: When $r_0 = 0, r_1 = \mp \frac{4\sqrt{6}b}{\sqrt{ac+2ad}}, a_1 = \mp \frac{4\sqrt{6}b}{\sqrt{a(c+2d)}}, s = -8b$, the exact traveling wave solutions are provided by

$$\Psi_{12}(x, t) = \pm \frac{4\sqrt{6} b \tanh(8bt + x) (\coth^2(8bt + x) + 1)}{\sqrt{a(c + 2d)}},$$

$$\Gamma_{12}(x, t) = -\frac{6 b (\tanh(8bt + x) + \coth(8bt + x))^2}{c + 2d}.$$

Cluster-4: When $r_0 = 0, r_1 = \mp \frac{2\sqrt{6}b}{\sqrt{ac+2ad}}, a_1 = 0, s = -2b$, exact traveling wave solutions are provided by

$$\Psi_{13}(x, t) = \pm \frac{2\sqrt{6} b \tanh(2bt + x)}{\sqrt{a(c + 2d)}}, \tag{14}$$

$$\Gamma_{13}(x, t) = -\frac{6 b \tanh^2(2bt + x)}{c + 2d}.$$

Family 2: For $v = [i, -i, 1, 1]$ and $k = [i, -i, i, -i]$, Equation (11) becomes

$$Y(\zeta) = -\frac{\sin \zeta}{\cos \zeta}. \tag{15}$$

The algebraic system is obtained by substituting Equation (15) into Equation (12) and then inserting the result into Equation (6). The solutions are as follows:

Cluster-1: When $r_0 = 0, r_1 = \mp \frac{4\sqrt{3}b}{\sqrt{ac+2ad}}, a_1 = \pm \frac{4}{3} \left(-\frac{2\sqrt{3}abc}{(a(c+2d))^{3/2}} - \frac{4\sqrt{3}abd}{(a(c+2d))^{3/2}} - \frac{\sqrt{3}b}{\sqrt{a(c+2d)}} \right), s = -4b$, the exact traveling wave solutions are provided by

$$\Psi_{14}(x, t) = \pm \frac{8\sqrt{3} b \csc(2(4bt + x))}{\sqrt{a(c + 2d)}},$$

$$\Gamma_{14}(x, t) = -\frac{24 b \csc^2(2(4bt + x))}{c + 2d}.$$

Cluster-2: When $r_0 = 0, r_1 = 0, a_1 = \mp \frac{2\sqrt{6}b}{\sqrt{-ac-2ad}}, s = 2b$, the exact traveling wave solutions are provided by

$$\Psi_{15}(x, t) = \mp \frac{2\sqrt{6} b \cot(2bt - x)}{\sqrt{-a(c + 2d)}},$$

$$\Gamma_{15}(x, t) = -\frac{6 b \cot^2(2bt - x)}{c + 2d}.$$

Cluster-3: When $r_0 = 0, r_1 = \mp \frac{2\sqrt{6}b}{\sqrt{-ac-2ad}}, a_1 = \pm \frac{2}{3} \left(-\frac{\sqrt{6}abc}{(-a(c+2d))^{3/2}} - \frac{2\sqrt{6}abd}{(-a(c+2d))^{3/2}} - \frac{\sqrt{6}b}{\sqrt{-a(c+2d)}} \right), s = 2b$, the exact traveling wave solutions are provided by

$$\Psi_{16}(x, t) = \mp \frac{2\sqrt{6} b \tan(2bt - x)}{\sqrt{-a(c + 2d)}},$$

$$\Gamma_{16}(x, t) = -\frac{6 b \tan^2(2bt - x)}{c + 2d}.$$

Cluster-4: When $r_0 = 0, r_1 = \pm \frac{4\sqrt{6}b}{\sqrt{-ac-2ad}}, a_1 = \mp \frac{4\sqrt{6}b}{\sqrt{-a(c+2d)}, s = 8b$, the exact traveling wave solutions are provided by

$$\Psi_{17}(x, t) = \mp \frac{4\sqrt{6} b \tan(8bt - x) (\cot^2(8bt - x) - 1)}{\sqrt{-a(c + 2d)}},$$

$$\Gamma_{17}(x, t) = -\frac{6 b (\cot(8bt - x) - \tan(8bt - x))^2}{c + 2d}.$$

3. Numerical Results

This section uses two techniques (uniform mesh and adaptive moving mesh methods) to obtain the numerical solutions to the system (1).

3.1. Numerical Solutions Using a Uniform Mesh

In this subsection, we use a fixed mesh technique on a physical domain of size $[0, L]$ to obtain numerical results for system (1). The domain is divided into N_x subintervals of uniform width $h = L/N_x$, denoted by $[x_j, x_{j+1}]$, where $x_j = (j - 1)h$ for all $x_j \in [0, L]$ and $j = 1, 2, \dots, N_x + 1$. To discretize system (1), we utilize the Crank–Nicolson method in the following manner:

$$\Gamma_t|_j^n + \frac{a}{2} [\Psi_j^{n+1} \Psi_x|_j^{n+1} + \Psi_j^n \Psi_x|_j^n] = 0,$$

$$\Psi_t|_j^n + \frac{b}{2} [\Psi_{xxx}|_j^{n+1} + \Psi_{xxx}|_j^n] + \frac{c}{2} [\Gamma_j^{n+1} \Psi_x|_j^{n+1} + \Gamma_j^n \Psi_x|_j^n] + \frac{d}{2} [\Psi_j^{n+1} \Gamma_x|_j^{n+1} + \Psi_j^n \Gamma_x|_j^n] = 0,$$

where

$$\Gamma_t|_j^n = \frac{\Gamma_j^{n+1} - \Gamma_j^n}{k}, \Psi_t|_j^n = \frac{\Psi_j^{n+1} - \Psi_j^n}{k}, \Psi_x|_j = \frac{\Psi_{j+1} - \Psi_{j-1}}{2h},$$

$$\Gamma_x|_j = \frac{\Gamma_{j+1} - \Gamma_{j-1}}{2h}, \Psi_{xxx}|_j = \frac{\Psi_{j+2} - 2\Psi_{j+1} + 2\Psi_{j-1} - \Psi_{j-2}}{2h^3},$$

the associated boundary conditions of system (1) are

$$\Gamma_{t,1} = \Gamma_{t,N_x+1} = 0,$$

$$\Psi_{t,1} = \Psi_{t,N_x+1} = 0,$$

the initial condition is selected by calculating Equation (14) at $t = 0$ as follows:

$$\Psi = \pm \frac{2\sqrt{6} b \tanh(x)}{\sqrt{a(c + 2d)}},$$

$$\Gamma = -\frac{6 b \tanh^2(x)}{c + 2d},$$

where a, b, c, d are constants.

3.1.1. Stability

In this section, we will assess the stability of the numerical solution by utilizing Fourier’s stability technique. To apply this technique, we first need to linearize Equation (5) as follows:

$$\Psi_t + b\Psi_{xxx} + D_0\Psi_x = 0, \tag{16}$$

where b and D_0 are constants, such that $D_0 = \alpha\Psi^2$. Fully discretize Equation (16) is given by

$$\Psi_j^{n+1} - \Psi_j^n = -b\frac{k}{2} [\Psi_{xxx}|_j^{n+1} + \Psi_{xxx}|_j^n] - D_0\frac{k}{2} [\Psi_x|_j^{n+1} + \Psi_x|_j^n]. \tag{17}$$

Let

$$\Psi_j^n = Y^n e^{i\zeta jh} \quad \text{and then} \quad \Psi_j^{n+1} = Y\Psi_j^n, \quad j = 1, 2, 3, \dots, N_x. \tag{18}$$

The following is the result of placing Equation (18) into the scheme (17):

$$Y\Psi_j^n - \Psi_j^n = -b\frac{k}{4h^3} [Ye^{2i\zeta h}\Psi_j^n - 2Ye^{i\zeta h}\Psi_j^n + 2Ye^{-i\zeta h}\Psi_j^n - Ye^{-2i\zeta h}\Psi_j^n + e^{2i\zeta h}\Psi_j^n - 2e^{i\zeta h}\Psi_j^n + 2e^{-i\zeta h}\Psi_j^n - e^{-2i\zeta h}\Psi_j^n] - D_0\frac{k}{4h} [Ye^{i\zeta h}\Psi_j^n - Ye^{-i\zeta h}\Psi_j^n + e^{i\zeta h}\Psi_j^n - e^{-i\zeta h}\Psi_j^n], \tag{19}$$

by dividing the two sides of Equation (19) by Ψ_j^n and taking Y as a common factor, we arrive at

$$Y - 1 = -\left(b\frac{k}{4h^3} \left(-8\sin(h\zeta)\sin^2\left(\frac{h\zeta}{2}\right)\right) + D_0\frac{k}{4h} 2i\sin(h\zeta)\right)(Y + 1),$$

let $\theta = b\frac{k}{4h^3} \left(-8\sin(h\zeta)\sin^2\left(\frac{h\zeta}{2}\right)\right) + D_0\frac{k}{4h} 2i\sin(h\zeta)$. Hence,

$$|Y| = \left|\frac{1 - \theta}{1 + \theta}\right| \leq 1, \tag{20}$$

according to the analysis and as demonstrated in Equation (20), the numerical scheme remains stable without any conditions as long as the absolute value of Y is not greater than one.

3.1.2. Error Analysis

In this section, we use the Taylor series to look at the order of accuracy, which necessitates the initial discretization of Equation (5)

$$\Psi_t|_j^n + \frac{b}{2} [\Psi_{xxx}|_j^{n+1} + \Psi_{xxx}|_j^n] + \frac{\alpha}{2} [\Psi_j^{n+1}\Psi_x|_j^{n+1} + \Psi_j^n\Psi_x|_j^n] = 0. \tag{21}$$

Next, we determine the order by evaluating the truncation error. Assume that

$$e_j^{n+1} = \Psi_j^{n+1} - \Psi(x_j, t_{n+1}), \tag{22}$$

where e_j^{n+1} represents the error, while Ψ_j^{n+1} and $\Psi(x_j, t_{n+1}) = \Psi$ represent the approximate and analytical solutions, respectively. Now, we substitute Equation (22) into Equation (21),

$$e_j^{n+1} = \frac{-bk}{2} \left[\frac{e_{j+2}^{n+1} - 2e_{j+1}^{n+1} + 2e_{j-1}^{n+1} - e_{j-2}^{n+1}}{2h^3} + \frac{e_{j+2}^n - 2e_{j+1}^n + 2e_{j-1}^n - e_{j-2}^n}{2h^3} \right] - \frac{\alpha k}{2} \left[e_j^{n+1} \left(\frac{e_{j+1}^{n+1} - e_{j-1}^{n+1}}{2h} \right) + e_j^n \left(\frac{e_{j+1}^n - e_{j-1}^n}{2h} \right) \right] + e_j^n + T_j^n, \tag{23}$$

where T_j^n represents the truncation error and is written as

$$T_j^n \leq \frac{k^2}{6} \Psi_{ttt} + \frac{7b}{40} h^2 \Psi_{xxxxx} + \frac{\alpha k^2 h^2}{24} \Psi_{tt}^2 \Psi_{xxx} + \frac{\alpha h^4}{240} \Psi \Psi_{xxxxx}, \tag{24}$$

consequently, the numerical scheme’s truncation error is

$$T_j^n = O(k^2, h^2).$$

3.1.3. Convergence

We need to refine two meshes with h and k values equaling zero to compute a sequence of computations using the initial data. Additionally, we must ensure that a convergent numerical scheme is used for every fixed point (x^*, t^*) within a selected domain $[a, b]$ and $[0, T_e]$,

$$x_j \rightarrow x^*, \quad t_n \rightarrow t^* \quad \text{implies} \quad \Psi_j^n = \Psi(x^*, t^*).$$

As previously mentioned, the numerical scheme is unconditionally stable. Now, we will demonstrate that these schemes are also unconditionally convergent. To do so, let us assume that the error e is defined as $e_j^n = \Psi_j^n - \Psi(x_j, t_n)$. Now, Ψ_j^n exactly satisfies the scheme described by Equation (21), while $\Psi(x_j, t_n)$ omits the error indicated by the truncation error kT_j

$$e_j^{n+1} = \frac{-bk}{2} \left[\frac{e_{j+2}^{n+1} - 2e_{j+1}^{n+1} + 2e_{j-1}^{n+1} - e_{j-2}^{n+1}}{2h^3} + \frac{e_{j+2}^n - 2e_{j+1}^n + 2e_{j-1}^n - e_{j-2}^n}{2h^3} \right] - \frac{\alpha k}{2} \left[e_j^{n+1} \left(\frac{e_{j+1}^{n+1} - e_{j-1}^{n+1}}{2h} \right) + e_j^n \left(\frac{e_{j+1}^n - e_{j-1}^n}{2h} \right) \right] + e_j^n + kT_j^n,$$

where T_j is the truncation error; see Equation (24). If we suppose that the maximum error for the time step is given by

$$E^n := \max \{ |e_j^n|, j = 1, 2, \dots, N_x - 1, n \geq 0 \}, \tag{25}$$

then substituting Equation (25) into Equation (23) yields

$$e_j^{n+1} \leq E^n + kT_j^n,$$

since the above inequality holds for each $j = 1, 2, \dots, N_x - 1$, we have

$$E^{n+1} \leq E^n + kT_j^n,$$

since the given initial data are used, we can identify $E_0 = 0$. Hence, the inequality is given by

$$E^n \leq n \times kT_j^n,$$

hence, the scheme described by Equation (21) is convergent as $h, k \rightarrow 0$.

3.2. Numerical Solutions Using an Adaptive Mesh

To obtain the numerical results of system (1), we employ the adaptive mesh method. The first step is to transform the physical domain $[0, L]$ into the computational domain $[0, 1]$ using the mapping $x = x(\eta, t) : [0, 1] \rightarrow [0, L], t > 0$. This transformation allows us to apply the proposed numerical technique. By using the physical coordinate x and the computational coordinate η , we can represent the solution as $\Psi = \Psi(x, t), \Gamma = \Gamma(x, t)$ where $x = x(\eta, t)$. When the coordinate x is rearranged, it becomes $x_j(\eta) = x(\eta_j, t)$ where $\eta_j = (j - 1)/N_x, j = 1, 2, 3, \dots, N_x + 1$. The MMPDE that is most frequently used is as follows:

$$\text{MMPDE5} : \tau(1 - \kappa \partial_{\eta\eta})x_t = \frac{1}{Q}(Qx_\eta)_\eta, \tag{26}$$

assuming that τ and κ are constants, we introduce the function $Q(\Gamma, \Psi, x)$, which is known as a monitor function. This function identifies regions in which the solution changes significantly, such as areas with large curvatures or high variations in the solution, and assigns more grid points to those regions. A commonly used monitor function, as proposed by Alharbi et al. [31], is given by

$$\text{The arc length} : Q(\Gamma, \Psi, x) = \sqrt{1 + \frac{\Gamma_\eta^2}{x_\eta^2} + \frac{\Psi_\eta^2}{x_\eta^2}}. \tag{27}$$

To apply the MMPDE5, we use the initial condition $x_j = (j - 1)L/N_x$ and the boundary conditions $x(0, t) = 0$ and $x(L, t) = L$. Additionally, the computational coordinate is denoted by $\eta_j = (j - 1)h_\eta$, where $h_\eta = L/N_x$ and $j = 1, 2, \dots, N_x + 1$. To discretize the physical domain, we divide it into N_x equal subintervals $x_0 < x_1 < x_2 < \dots < x_{N_x}$. We then apply the chain rule to system (1) and obtain:

$$\begin{aligned} \Gamma_t - \left(\frac{\Gamma_\eta}{x_\eta}\right)x_t &= -a\Psi\left(\frac{\Psi_\eta}{x_\eta}\right), \\ \Psi_t - \left(\frac{\Psi_\eta}{x_\eta}\right)x_t &= -b\frac{1}{x_\eta}\left(\frac{1}{x_\eta}\left(\frac{\Psi_\eta}{x_\eta}\right)_\eta\right) - c\Gamma\left(\frac{\Psi_\eta}{x_\eta}\right) - d\Psi\left(\frac{\Gamma_\eta}{x_\eta}\right), \end{aligned} \tag{28}$$

with boundary conditions

$$\begin{aligned} \Gamma_{t,1} = \Gamma_{t,N_x+1} &= 0, \\ \Psi_{t,1} = \Psi_{t,N_x+1} &= 0, \end{aligned} \tag{29}$$

the initial condition is selected by calculating Equation (14) at $t = 0$ as follows:

$$\begin{aligned} \Psi &= \pm \frac{2\sqrt{6} b \tanh(x)}{\sqrt{a(c + 2d)}}, \\ \Gamma &= -\frac{6 b \tanh^2(x)}{c + 2d}, \end{aligned} \tag{30}$$

where a, b, c, d are constants. To clarify, the spatial derivative is semi-discretized while the temporal derivative remains continuous. This means that the problem described in system (1) becomes a set of ordinary differential equations, which can be solved using line methods. We use the MATLAB ODE solver (ode15i) to numerically integrate the resulting system. The discretization of Equation (28) must be achieved using finite differences in the following manner:

$$\begin{aligned} \Gamma_t - \frac{\Gamma_{j+1} - \Gamma_{j-1}}{x_{j+1} - x_{j-1}}x_t &= -a\Psi_{j+\frac{1}{2}}^2 \frac{\Psi_{j+1} - \Psi_{j-1}}{x_{j+1} - x_{j-1}}, \\ \Psi_t - \frac{\Psi_{j+1} - \Psi_{j-1}}{x_{j+1} - x_{j-1}}x_t &= -b\frac{\Psi_{xx,j+1} - \Psi_{xx,j}}{x_{j+1} - x_{j-1}} - c\Gamma_{j+\frac{1}{2}} \frac{\Psi_{j+1} - \Psi_{j-1}}{x_{j+1} - x_{j-1}} - d\Psi_{j+\frac{1}{2}} \frac{\Gamma_{j+1} - \Gamma_{j-1}}{x_{j+1} - x_{j-1}}, \end{aligned} \tag{31}$$

where

$$\Psi_{xx,j} = \frac{2}{x_{j+1} - x_{j-1}} \left[\frac{\Psi_{j+1} - \Psi_j}{x_{j+1} - x_j} - \frac{\Psi_j - \Psi_{j-1}}{x_j - x_{j-1}} \right], \Psi_{j+\frac{1}{2}} = \frac{\Psi_{j+1} + \Psi_j}{2}, \Gamma_{j+\frac{1}{2}} = \frac{\Gamma_{j+1} + \Gamma_j}{2}.$$

3.3. Results and Discussion

Significant results have been achieved through the successful use of the GERFM and MVNK methods in extracting multiple exact solutions for Equation (5) in this study. It is important to mention that Equation (5) was obtained by converting the coupled Drinfel’d–Sokolov–Wilson system (1). Figures 1 and 2 display the exact solutions for $\Psi_2(x, t)$ and $\Gamma_2(x, t)$ for Equation (5). In Figure 1a,b, we used the MVNK method to create 3D plots of the analytical solution for Equation (5). Meanwhile, in Figure 2c,d, we also utilized the MVNK method to obtain 3D plots of the analytical solution for Equation (5). The parameters utilized are $b = 1, a = 0.4, c = 0.5, d = 0.7,$ and $N = 1000$. Figure 3a,b demonstrate the behavior of waves when one parameter is changed while keeping others constant. The parameter being modified in this case is b , which affects both the direction and amplitude of the waves. It is apparent that when b is negative, the wave direction is always negative.

This article additionally investigates the numerical solutions of the coupled Drinfel’d–Sokolov–Wilson system (1) through the utilization of two numerical methodologies: the uniform mesh and the adaptive moving mesh methods. The results obtained are precise and efficient. The results in Figures 4–6 exhibit oscillations, but the adaptive moving mesh method effectively minimizes errors and produces acceptable results without oscillations.

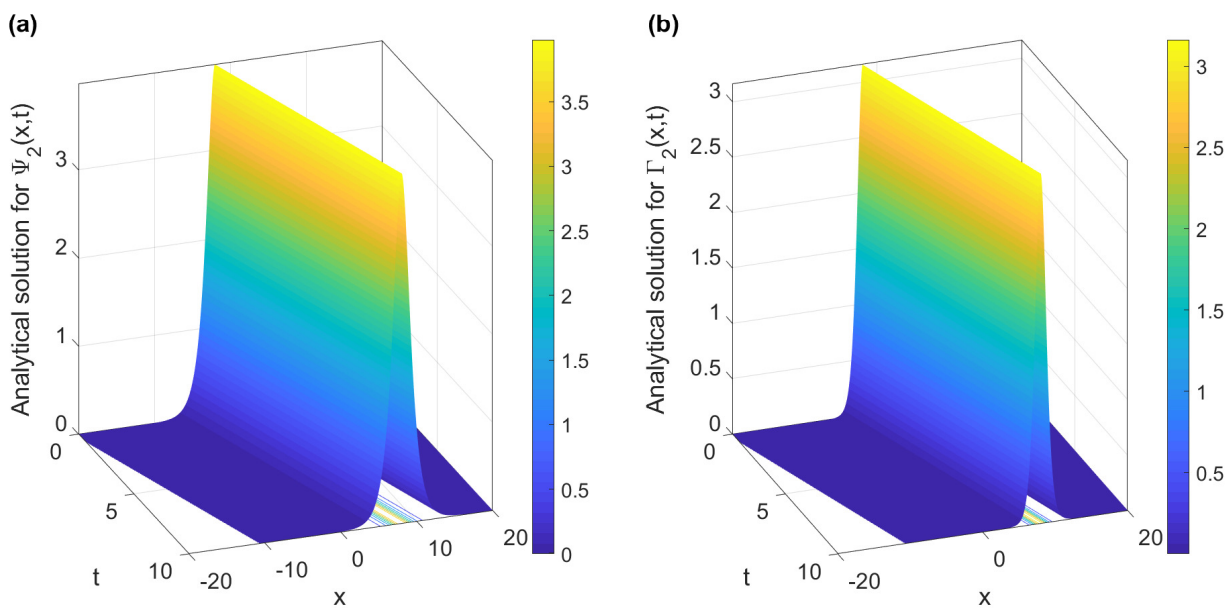


Figure 1. The MVNK method was used to obtain 3D plots of the analytical solution to Equation (5). The parameters are given by (a,b) $b = 1, a = 0.4, c = 0.5, d = 0.7, x_0 = 2$ with $t = 0 \rightarrow 10$ and $x = -20 \rightarrow 20$.

The study presents numerical results from time $t = 0 \rightarrow 10$. As shown in Figure 4a,b, the adaptive moving mesh approach demonstrates more significant agreement with the analytical solution than the uniform approach. The insets in Figure 4a,b provide a closer look at the steep front regions of the plot. These regions are characterized by a rapid change in values and require a higher density of points for accurate representation. In the insets, these areas are indicated by yellow circles, indicating the need for more data points in those specific regions. As a result, the outcomes for both $\Psi(x, t)$ and $\Gamma(x, t)$ seem almost

identical in these regions. Figure 4c depicts the obtained values of $x = (\eta, t)$ using the MMPDE5 Equation (26) along with the monitor function Equation (27). The parameters employed for this calculation are as follows: $b = 1, a = 1, c = 1, d = 1, x_0 = -10$, with $N_x = 800, L = 20$, and $t = 10$. These figures demonstrate that the monitor function sends additional points to areas with $\Delta x = 5 \times 10^{-5}$ curvatures while reducing the mesh points in other regions with $\Delta x = 5 \times 10^{-2}$ (where Δx is the distance between points). The initial uniform mesh is set to $\Delta x = 1 \times 10^{-3}$ across all areas. Furthermore, it can be observed from Figure 4 that the numerical solutions obtained using a uniform mesh exhibit excellent agreement with the analytical solution. However, it is worth noting that achieving this level of accuracy requires a very small value of Δx . Also, Figure 4 shows that numerical solutions achieved through a uniform mesh require a value of $N_x = 10,000$ to display excellent agreement with the analytical solution. On the other hand, adaptive moving mesh only requires $N_x = 1000$ to exhibit excellent agreement with the analytical solution.

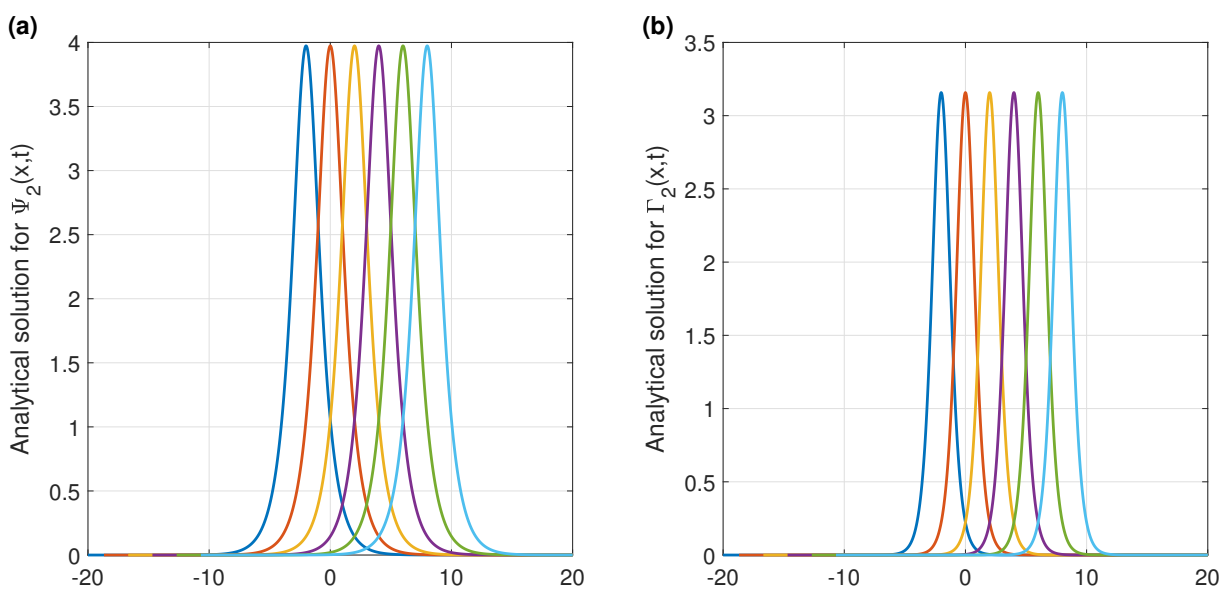


Figure 2. The MVNK method was used to obtain 2D plots of the analytical solution to Equation (5). The parameters are given by (a,b) $b = 1, a = 0.4, c = 0.5, d = 0.7, x_0 = 2$ with $t = 0 \rightarrow 10$ and $x = -20 \rightarrow 20$.

It is important to mention that the mesh is redistributed through the use of a monitor function that regulates its evaluation. The monitor function choice has a big impact on how the mesh moves. To prevent mesh tangles that often occur with mesh distribution, a special function called spatial smoothing is used.

Figures 5 and 6 show the results of an analysis that compared the solitary waves of an analytical solution Equation (5) and a numerical solution that uses an adaptive moving mesh. In Figure 5, 3D surface plots depict the analytical solutions for Ψ_{13} and Γ_{13} in (a) and (c), while (b) and (d) show the numerical solutions. The analysis used the following parameters: $b = 1, a = 1, c = 1, d = 1, x_0 = -10$, with $N_x = 10,000$, and $t = 0 \rightarrow 10$. Figure 6 shows 2D plots of the same solutions. The analytical solutions for Ψ_{13} and Γ_{13} are depicted in (a) and (c), while the numerical solutions are shown in (b) and (d). These figures offer sufficient evidence that the numerical and analytic solutions are highly similar. The clear implication is that the adaptive moving mesh method surpasses the uniform mesh approach in terms of accuracy, reliability, and convergence. This study’s methods can be used to investigate other NPDEs.

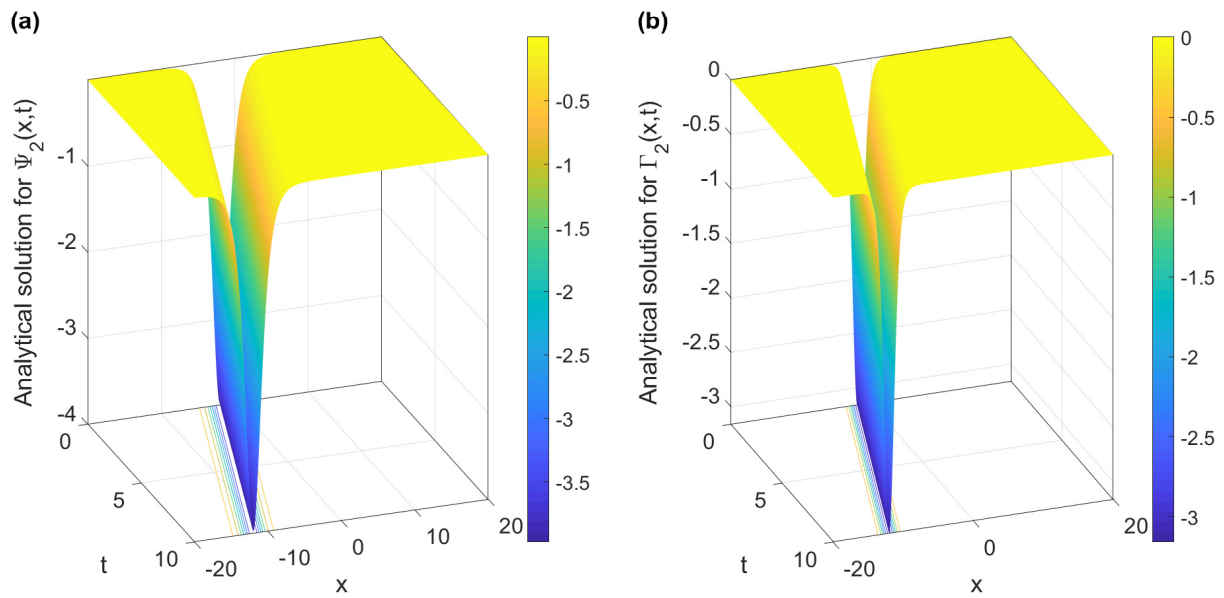


Figure 3. The MVNK method was used to obtain 3D plots of the analytical solutions to Equation (5). The parameters are given by (a,b) $b = -1, a = 0.4, c = 0.5, d = 0.7, x_0 = 2$ with $N = 1000, t = 0 \rightarrow 10$ and $x = -20 \rightarrow 20$.

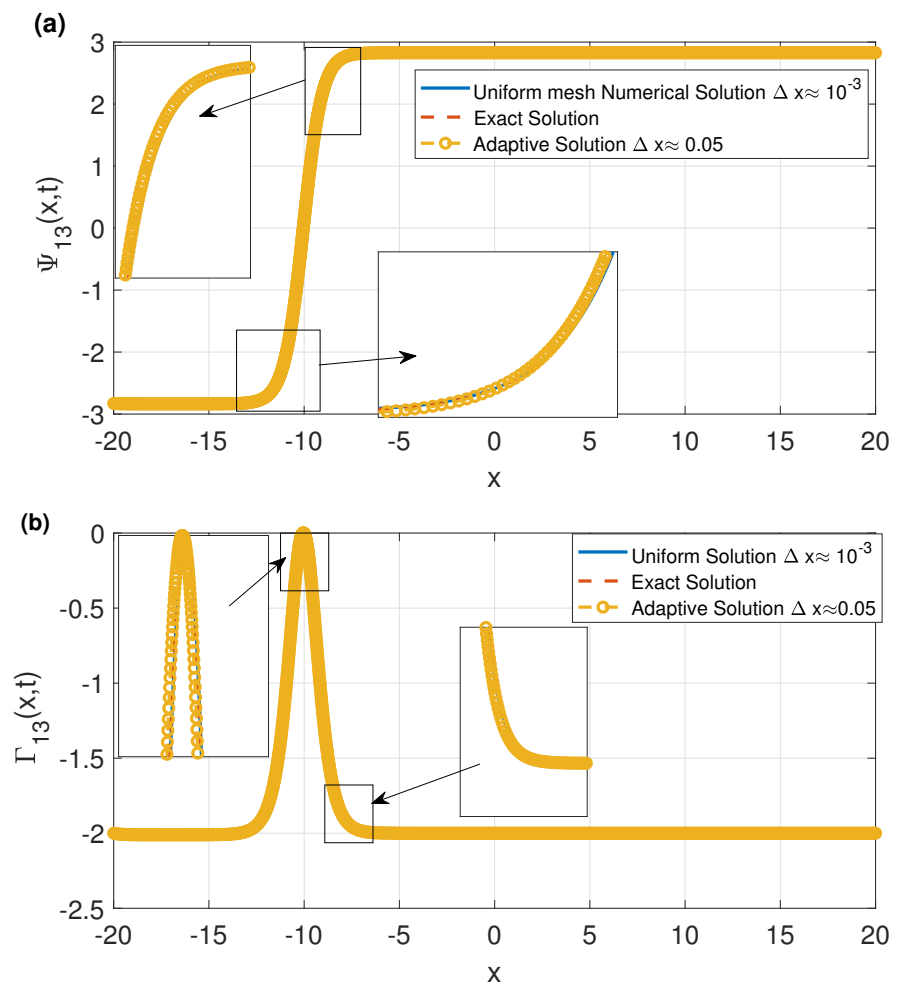


Figure 4. Cont.

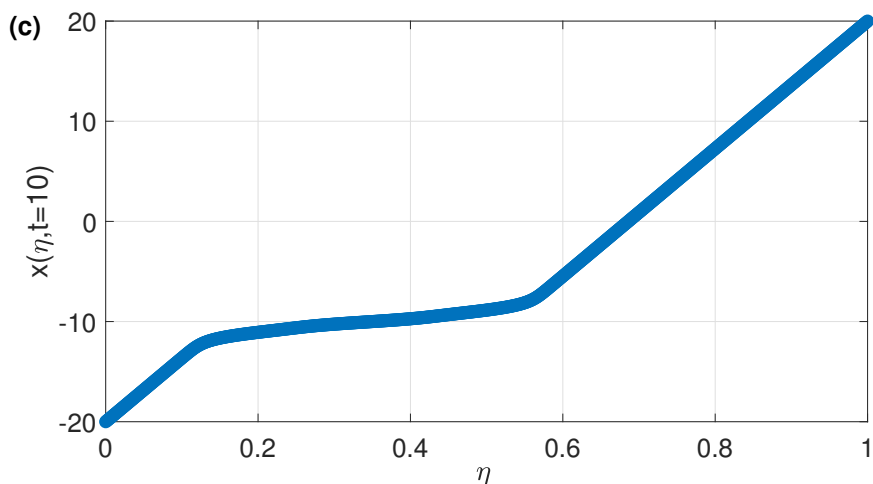


Figure 4. The comparison between the exact solutions obtained through Equation (5) and the numerical results obtained using both an adaptive moving mesh and a uniform mesh is made in (a,b). In (c), the mesh obtained by applying MMPDE5 and the monitor function is plotted. The following parameters were used: $a = 1, b = 1, c = 1, d = 1, x_0 = -10, L = 20, N = 800,$ and $t = 10$.

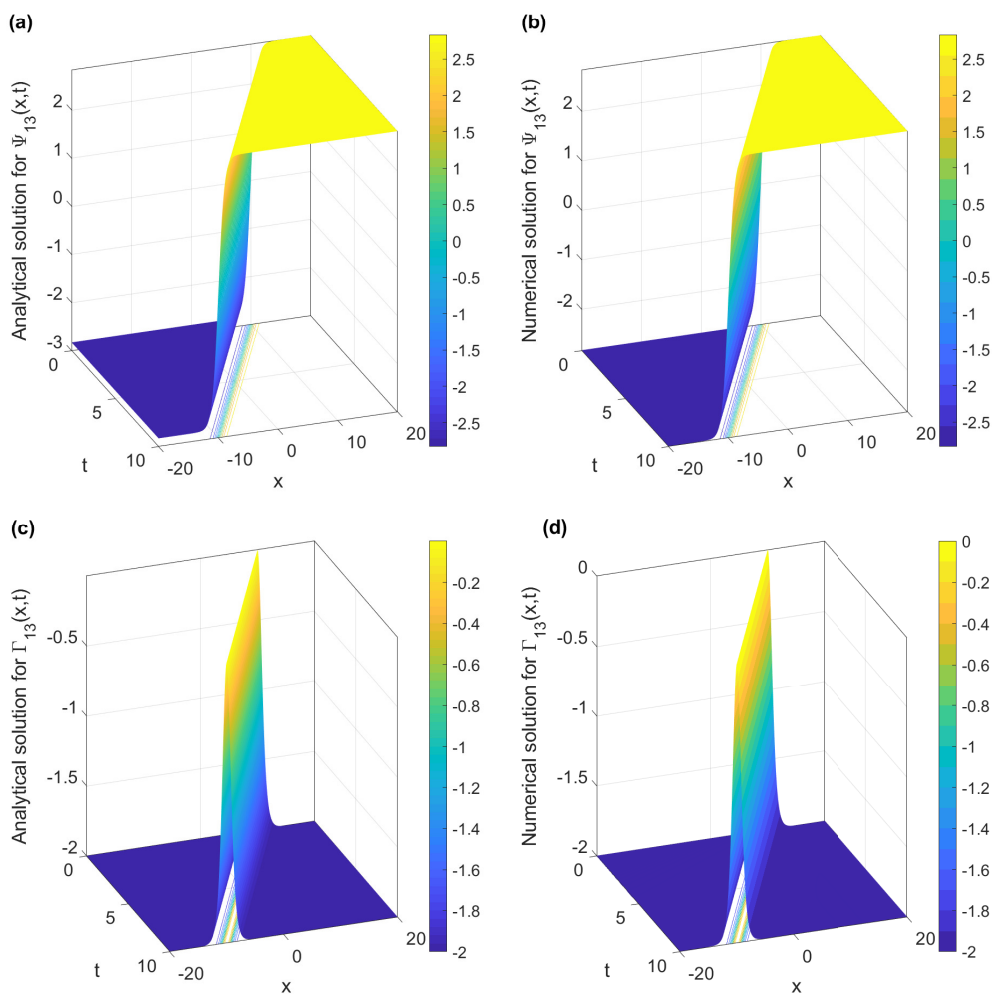


Figure 5. The GERFM method method was used to find the analytical solution for Ψ_{13} and Γ_{13} , as shown in (a,c) as 3D surface plots; (b,d) show the adaptive moving mesh numerical solution results. The study parameters are $b = 1, a = 1, c = 1, d = 1, x_0 = -10,$ with $t = 0 \rightarrow 10$ and $x = -20 \rightarrow 20$.

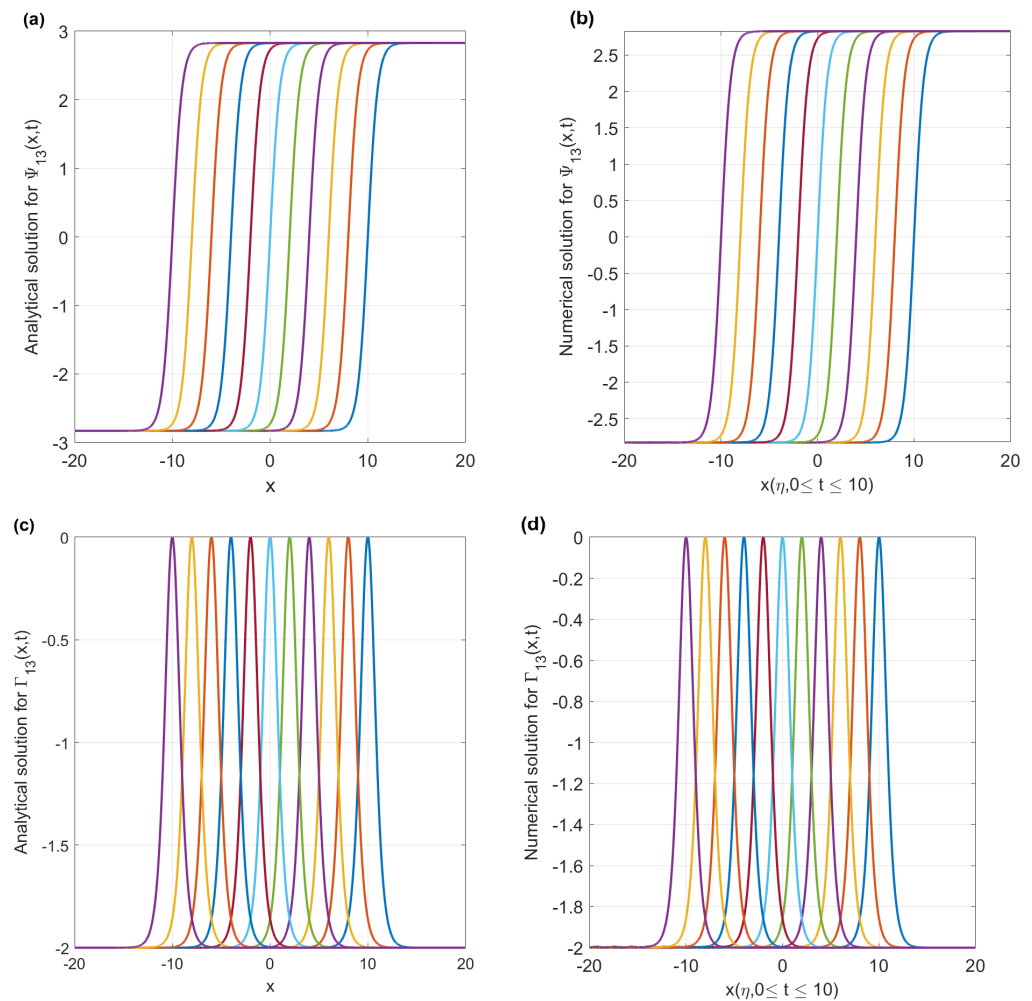


Figure 6. The GERFM method was used to find the analytical solution for Ψ_{13} and Γ_{13} , as shown in (a,c) as 2D plots; (b,d) show the adaptive moving mesh numerical solution results. The study parameters are $b = 1, a = 1, c = 1, d = 1, x_0 = -10$, with $t = 0 \rightarrow 10$ and $x = -20 \rightarrow 20$.

4. Conclusions

In this study, we used the GERFM and MVNK methods to find some new traveling wave solutions for Equation (5) by expressing them in trigonometric and hyperbolic functions. We also employed the adaptive moving mesh method and uniform mesh to obtain numerical solutions while reducing the associated error. We observed that our methods yield superior outcomes compared to the cosine function approach. Previous studies on the coupled Drinfel’d–Sokolov–Wilson system mainly focused on generating numerical solutions without addressing error reduction. However, our study has successfully obtained numerical solutions while reducing the associated error. We found that the adaptive mesh approach is more reliable than the uniform mesh approach. Our results show that the adaptive mesh method effectively distributes points in regions with higher error. We also created 2D and 3D figures to illustrate the effectiveness of the employed approaches. Also, the investigation reveals that scheme (17) is second-order accurate in both k^2 and h^2 , and the scheme is unconditionally stable. Overall, the exact and numerical methods used in this study are flexible and effective in developing specific traveling wave solutions for nonlinear PDEs.

It is evident from the presented figures that the precise solutions exhibit similar characteristics to the numerical answers. Furthermore, the efficacy of the employed methodologies is clearly demonstrated in Table 1 and Figure 7. The table presents the L_2 error and CPU time required to achieve a time value of $t = 10$ using the adaptive approach. The initial

number of points, N_x , was set to 200. The L_2 error was observed to gradually converge towards a value of approximately 10^{-5} , which is often considered acceptable in this context. The inaccuracy exhibits a significant decrease with the increase in the number of points. However, there is a slight increase in the CPU time as the number of points increases. For example, when the sample size is equal to $N_x = 1600$, the L_2 error reaches a value of 1.85×10^{-5} during a duration of $t = 10$ min. The marginal increase in CPU time can be attributed to the fact that the utilized functions are computed within the process. Moreover, Figure 7 illustrates a significant decrease in the relative error for Ψ and Γ as the number of points increases. The rate of error reduction is swift due to the adaptive process, which effectively provides the locations with high error with an ample and appropriate number of points. As a result, the adaptive technique demonstrates an increased processing capacity and applicability in the resolution of nonlinear partial differential equations.

Table 1. The convergence histories using L_2 norm at $t = 10$.

N_x	The Relative Error (Ψ)	The Relative Error (Γ)
200	9.20×10^{-4}	1.00×10^{-3}
400	2.51×10^{-4}	5.03×10^{-4}
800	7.11×10^{-5}	1.43×10^{-4}
1600	1.85×10^{-5}	3.75×10^{-5}
2000	1.10×10^{-5}	2.22×10^{-5}

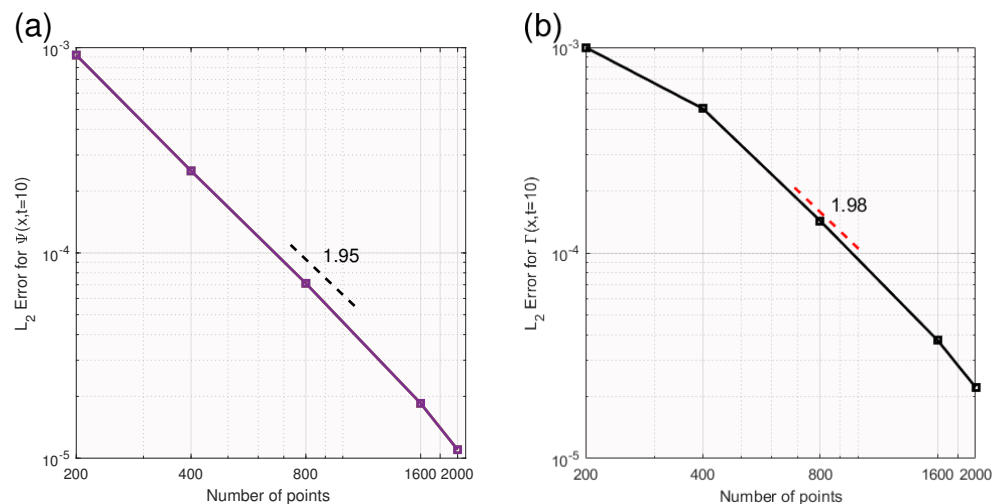


Figure 7. This figures (a,b) show the convergence histories using L_2 norm as a function of the number of points N_x . The parameters are given by $a = 1, b = 1, c = 1, d = 1, x_0 = -10, L = 20, N = 800$, and $t = 10$.

It has been observed that numerical systems with more mesh points are more precise than those with fewer mesh points but have more significant differences. By examining the crucial aspects of the solution’s behavior, it was found that the non-uniform mesh can produce more accurate results than a fixed uniform mesh. Increasing the number of mesh points in the non-uniform mesh can improve its precision, but it requires additional time to solve partial differential equations. For example, when the number of points in the x direction is increased from 200 to approximately 1000, a non-uniform mesh is considerably faster than a fixed uniform mesh. This improvement in CPU time is more beneficial when the desired accuracy is low enough. Implicit non-uniform mesh schemes have shown promise in some problems due to their efficiency and ease of implementation, outperforming fixed uniform mesh schemes and h or hp -adaptive methods. But to keep the uniform mesh from becoming tangled up and disorganized, we need to look into different ways to make meshes in non-uniform frameworks. These techniques include the adaptive moving mesh method and optimal transport equations such as the Monge–Ampère and

parabolic Monge-Ampère equations, which can generate regular meshes without tangling. Testing these techniques on more complex two-dimensional problems is necessary to ensure their viability. The numerical resolution of the problem becomes challenging and computationally demanding for the interior layers related to the capillary ridge region. Hence, the solution to the two-dimensional equations has been effectively obtained using the non-uniform moving mesh approach, which relies on moving mesh partial differential equations. The study's findings indicate that this approach holds significant promise for addressing nonlinear equations on a large scale, but further testing is required to confirm its potential for success.

Author Contributions: Methodology, S.H.A.; software, A.A.; formal analysis, A.A.; investigation, S.H.A.; resources, S.H.A. and A.A.; supervision, A.A. All authors have read and agreed to the published version of the manuscript.

Funding: The authors wish to express their gratitude to the Deanship for Research and Innovation at the Ministry of Education in Saudi Arabia for funding this research under project number 445-9-550.

Data Availability Statement: The datasets generated during and/or analysed during the current study are available from the corresponding author on reasonable request.

Conflicts of Interest: The authors declare no conflict of interest.

References

- Li, T.; Vigiialoro, G. Analysis and Explicit Solvability of Degenerate Tensorial Problems. *Bound. Value Probl.* **2018**, *2018*, 2. [[CrossRef](#)]
- Lu, D.; Seadawy, A.R.; Ali, A. Dispersive Analytical Wave Solutions of Three Nonlinear Dynamical Water Waves Models via Modified Mathematical Method. *Results Phys.* **2019**, *13*, 102177. [[CrossRef](#)]
- Shen, S.; Yang, Z.; Li, X. Periodic Propagation of Complex-Valued Hyperbolic-Cosine-Gaussian Solitons and Breathers with Complicated Light Field Structure in Strongly Nonlocal Nonlinear Media. *Commun. Nonlinear Sci. Numer. Simul.* **2021**, *103*, 106005. [[CrossRef](#)]
- Shen, S.; Yang, Z.; Pang, Z.; Ge, Y. The Complex-Valued Astigmatic Cosine-Gaussian Soliton Solution of the Nonlocal Nonlinear Schrödinger Equation and Its Transmission Characteristics. *Appl. Math. Lett.* **2022**, *125*, 107755. [[CrossRef](#)]
- Song, L.; Yang, Z.; Li, X. Coherent Superposition Propagation of Laguerre-Gaussian and Hermite-Gaussian Solitons. *Appl. Math. Lett.* **2020**, *102*, 106114. [[CrossRef](#)]
- Zou, Z.; Guo, R. The Riemann-Hilbert Approach for the Higher-Order Gerdjikov-Ivanov Equation, Soliton Interactions and Position Shift. *Commun. Nonlinear Sci. Numer. Simul.* **2023**, *124*, 107316. [[CrossRef](#)]
- Nasreen, N.; Seadawy, A.R.; Lu, D.; Arshad, M. Construction of Modulation Instability Analysis and Optical Soliton Solutions of Perturbed Nonlinear Schrödinger Dynamical Equation with Power Law Nonlinearity in Non-Kerr Medium. *Results Phys.* **2019**, *13*, 102263. [[CrossRef](#)]
- Shehzad, K.; Seadawy, A.R.; Wang, J.; Arshad, M. Multi Peak Solitons and Breather Types Wave Solutions of Unstable NLSEs with Stability and Applications in Optics. *Opt. Quantum Electron.* **2022**, *55*, 7. [[CrossRef](#)]
- Wazwaz, A. Completely Integrable Coupled KdV and Coupled KP Systems. *Commun. Nonlinear Sci. Numer. Simul.* **2010**, *15*, 2828–2835. [[CrossRef](#)]
- Hao, W. An Adaptive Homotopy Tracking Algorithm for Solving Nonlinear Parametric Systems with Applications in Nonlinear ODEs. *Appl. Math. Lett.* **2022**, *125*, 107767. [[CrossRef](#)]
- Kumar, D.; Seadawy, A.R.; Joardar, A.K. Modified Kudryashov Method via New Exact Solutions for Some Conformable Fractional Differential Equations Arising in Mathematical Biology. *Chin. J. Phys.* **2018**, *56*, 75–85. [[CrossRef](#)]
- Bekir, A.; Ünsal, Ö. Analytic Treatment of Nonlinear Evolution Equations Using First Integral Method. *Pramana* **2012**, *79*, 3–17. [[CrossRef](#)]
- Chen, B.; Chen, B.; Zhao, H. A New Generalized Algebraic Method and Its Application in Nonlinear Evolution Equations with Variable Coefficients. *Z. Naturforschung* **2005**, *60*, 211–220. [[CrossRef](#)]
- Aasaraai, A. The Application of Modified F-Expansion Method Solving the MacCari's System. *Br. J. Math. Comput. Sci.* **2015**, *11*, 1–14. [[CrossRef](#)]
- Shi-Kuo, L.; Fu, Z.; Liu, S.; Zhao, Q. Jacobi Elliptic Function Expansion Method and Periodic Wave Solutions of Nonlinear Wave Equations. *Phys. Lett.* **2001**, *289*, 69–74. [[CrossRef](#)]
- Alharbi, A.; Almatrafi, M.B.; Seadawy, A.R. Construction of the Numerical and Analytical Wave Solutions of the Joseph-Egri Dynamical Equation for the Long Waves in Nonlinear Dispersive Systems. *Int. J. Mod. Phys. B* **2020**, *34*, 2050289. [[CrossRef](#)]
- Kupershmidt, B.A. Lie Algebras and Korteweg-de Vries Equations. *Phys. D Nonlinear Phenom.* **1987**, *27*, 294–310. [[CrossRef](#)]
- Liu, C.; Liu, X. Exact Solutions of the Classical Drinfel'd-Sokolov-Wilson Equations and the Relations among the Solutions. *Phys. Lett.* **2002**, *303*, 197–203. [[CrossRef](#)]

19. Zhao, X.; Zhi, H. An Improved F-Expansion Method and Its Application to Coupled Drinfel'd–Sokolov–Wilson Equation. *Commun. Theor. Phys.* **2008**, *50*, 309–314. [[CrossRef](#)]
20. İnç, M. On Numerical Doubly Periodic Wave Solutions of the Coupled Drinfel'd–Sokolov–Wilson Equation by the Decomposition Method. *Appl. Math. Comput.* **2006**, *172*, 421–430. [[CrossRef](#)]
21. Ren, B.; Lou, Z.-M.; Liang, Z.-F.; Tang, X. Nonlocal Symmetry and Explicit Solutions for Drinfel'd–Sokolov–Wilson System. *Eur. Phys. J. Plus* **2016**, *131*, 441. [[CrossRef](#)]
22. Misırlı, E.; Gürefe, Y. Exp-Function Method for Solving Nonlinear Evolution Equations. *Math. Comput. Appl.* **2011**, *16*, 258–266. [[CrossRef](#)]
23. Sahoo, S.; Ray, S.S. New Double-Periodic Solutions of Fractional Drinfeld–Sokolov–Wilson Equation in Shallow Water Waves. *Nonlinear Dyn.* **2017**, *88*, 1869–1882. [[CrossRef](#)]
24. Bibi, S.; Mohyud-Din, S.T. New Traveling Wave Solutions of Drinfeld–Sokolov–Wilson Equation Using Tanh and Extended Tanh Methods. *J. Egypt. Math. Soc.* **2014**, *22*, 517–523. [[CrossRef](#)]
25. Al-Askar, F.M.; Cesarano, C.; Mohammed, W.W. The Analytical Solutions of Stochastic-Fractional Drinfel'd–Sokolov–Wilson Equations via (\hat{G}/G) -Expansion Method. *Symmetry* **2022**, *14*, 2105. [[CrossRef](#)]
26. Al-Askar, F.M.; Mohammed, W.W.; Samura, S.K.; El-Morshedy, M. The Exact Solutions for Fractional-Stochastic Drinfeld–Sokolov–Wilson Equations Using a Conformable Operator. *J. Funct. Spaces* **2022**, *2022*, 1–9. [[CrossRef](#)]
27. Meral, G. Numerical Solution of Drinfel'd Sokolov Wilson System Using Differential Quadrature and Finite Difference Methods. *Karaelmas Sci. Eng. J.* **2019**, *9*, 232–236. [[CrossRef](#)]
28. Islam, S.; Wang, H. Some Analytical Soliton Solutions of the Nonlinear Evolution Equations. *J. Ocean. Eng. Sci.* **2022**. [[CrossRef](#)]
29. Alharbi, A. A Study of Traveling Wave Structures and Numerical Investigation of Two-Dimensional Riemann Problems with Their Stability and Accuracy. *Cmes-Comput. Model. Eng. Sci.* **2023**, *134*, 2193–2209. [[CrossRef](#)]
30. Ghanbari, B.; Yusuf, A.; İnç, M.; Băleanu, D. The New Exact Solitary Wave Solutions and Stability Analysis for the $(2 + 1) (2 + 1)$ -Dimensional Zakharov–Kuznetsov Equation. *Adv. Differ. Equ.* **2019**, *2019*, 49. [[CrossRef](#)]
31. Alharbi, A.R. Numerical Solution of Thin-Film Flow Equations Using Adaptive Moving Mesh Methods. Keele University, 2016. Available online: <https://eprints.keele.ac.uk/id/eprint/2356> (accessed on 1 March 2016).

Disclaimer/Publisher's Note: The statements, opinions and data contained in all publications are solely those of the individual author(s) and contributor(s) and not of MDPI and/or the editor(s). MDPI and/or the editor(s) disclaim responsibility for any injury to people or property resulting from any ideas, methods, instructions or products referred to in the content.